Magnetic local time dependency of radiation belt electron precipitation: impact on polar ozone

Pekka T. Verronen[1,2], Daniel R. Marsh[3,4], Monika E. Szeląg[2], and Niilo Kalakoski[2]

[1]Sodankylä Geophysical Observatory, University of Oulu, Sodankylä, Finland
[2]Space and Earth Observation Centre, Finnish Meteorological Institute, Helsinki, Finland
[3]Atmospheric Chemistry Observations and Modeling, National Center for Atmospheric Research, Boulder, CO, USA
[4]Priestley International Centre for Climate, University of Leeds, Leeds, UK

Correspondence: P .T. Verronen (pekka.verronen@oulu.fi)

Abstract. The radiation belts are regions in the near-Earth space where solar wind electrons are captured by the Earth's magnetic field. A portion of these electrons is continuously lost into the atmosphere where they cause ionisation and chemical changes. Driven by solar activity, electron forcing leads to ozone variability in the polar regions. Understanding possible dynamical connections to regional climate is an on-going research activity which supports the assessment of greenhouse gas

5   driven climate change by better definition of the solar-driven variability. In the context of the Coupled Model Intercomparison Project Phase 6 (CMIP6), energetic electron and proton precipitation is included in the solar forcing recommendation for the first time. For radiation belt electrons, CMIP6 forcing is from a daily, zonal mean proxy model. This zonal mean model ignores the well-known dependency of precipitation on magnetic local time (MLT), i.e. its diurnal variability. Here we use the Whole Atmosphere Community Climate Model with lower ionospheric chemistry extension (WACCM-D) to study the effect

10   of MLT dependency of electron forcing on the polar ozone response. We analyse simulations applying MLT-dependent and MLT-independent forcings, and contrast ozone responses in monthly mean data as well as in monthly means of individual local time sectors. We consider two cases: 1) year 2003 and 2) extreme, long-duration forcing. Our results indicate that the ozone responses to MLT-dependent and MLT-independent forcings are very similar, and the differences found are small compared to those related to overall uncertainties in electron forcing. We conclude that electron forcing that ignores the MLT dependency

15   will still provide an accurate ozone response in long-term climate simulations.

1 Introduction

Energetic particle precipitation (EPP) and its impact on middle atmospheric polar ozone is recognized as a potential driver for dynamical connections between space weather and regional climate variability (Andersson et al., 2014, and references therein). For the the Coupled Model Intercomparison Project Phase 6 (CMIP6), EPP is included for the first time in the recommended

20   solar forcing data set (Matthes et al., 2017). CMIP6 EPP set includes ionization in the troposphere-stratosphere-mesosphere-lower thermosphere due to solar protons ($1-300$ MeV), mid-energy electrons ($E = 30-1000$ keV), and galactic cosmic rays. Auroral electrons affecting thermospheric altitudes can be included in high-top models using CMIP6 record of geomagnetic indices Ap and Kp, while models with upper altitude limit at $\approx$80 km can use an upper boundary for EPP-produced odd

nitrogen. The combined EPP forcing time series is based on measurements, proxy models, reconstructions, and repetition of

25 historical solar cycles. For climate simulations, past and future, it provides a continuous data set from 1850 to 2300, and is

publicly available from the SPARC SOLARIS-HEPPA website (https://solarisheppa.geomar.de/cmip6, accessed in December

2019).

In the CMIP6 EPP data set, ionization rates due to mid-energy electrons (MEE) have been calculated using a precipitation

model driven by the geomagnetic Ap index (van de Kamp et al., 2016). This model is based on electron flux observations

30 of the Medium-Energy Proton and Electron Detectors (MEPED) flying aboard the Polar Operational Environmental Satellites

(POES). It provides daily, zonal average ionization rates. Thus, the model neglects diurnal variation in MLT which can reach

to several orders of magnitude, e.g. in the MEPED measurements (Horne et al., 2009; Whittaker et al., 2014).

Due to the energy range used for MEE, i.e. $E = 30 - 1000$ keV, the bulk of ionization affects the mesosphere at altitudes

from 90 to 60 km, corresponding to pressure levels $\approx 0.001 - 0.1$ hPa (van de Kamp et al., 2016). At these altitudes, EPP

35 causes ozone depletion through ionization, production of odd hydrogen ($HO_x = H + OH + HO_2$), and HO_x-driven catalytic

loss reaction cycles. Odd nitrogen ($NO_x = N + NO + NO_2$) is produced and enhanced as well, which can increase the HO_x-

driven mesospheric ozone depletion by changing the partitioning between HO_x species (Verronen and Lehmann, 2015). In

polar winter, NO_x loss through photodissociation is diminished and enhanced amounts can be transported to from mesosphere

to stratosphere inside the polar vortex (Callis and Lambeth, 1998; Siskind et al., 2000; Funke et al., 2005; Randall et al.,

40 2009; Päivärinta et al., 2016). This leads to ozone depletion in the upper stratosphere through NO_x-driven catalytic loss cycles,

typically in late winter and spring (Fytterer et al., 2015; Damiani et al., 2016).

EPP-related production of odd hydrogen arises from H_2O dissociation in reaction sequences forming positive cluster ions,

such as $H^+(H_2O)$, and is also linked to production of HNO_3 through negative ion chemistry (Verronen and Lehmann, 2013). In

addition to HO_x, efficient catalytic loss of ozone requires atomic oxygen which is abundant in the daytime mesosphere. Several

45 studies have reported a diurnal variability in the efficiency of HO_x production and magnitude of mesospheric ozone depletion

during EPP (Solomon et al., 1981; Aikin and Smith, 1999; Verronen et al., 2005, 2006; Verronen and Lehmann, 2013). This

variability is dependent on HO_x, atomic oxygen, and electron/negative ion ratio which have diurnal cycle in the mesosphere.

HO_x production efficiency also increases with larger amounts of H_2O and decreases with increasing EPP ionization.

Considering the diurnal variability of ozone depletion reported earlier, it seems clear that MLT-dependency of the MEE forc-

50 ing must be important if ozone data are analysed at a temporal resolution finer than a day. However, the CMIP6 MEE forcing

is intended for multi-decadal climate simulations which are typically analysed on longer time scales, e.g. as monthly averages.

Due to the complexity of factors affecting ozone depletion, it is not clear if results of such analysis are significantly dependent

on the diurnal variability of the EPP forcing. Understanding this would be essential because an accurate representation of

middle atmospheric ozone is crucially needed in climate simulations.

55 In this paper, we study the importance of the MLT dependency of the MEE forcing. We do this by comparing atmospheric

simulations with daily zonal mean MEE, i.e. CMIP6 style forcing, to simulations using MLT-dependent MEE. An updated

version of the MEE precipitation model includes the dependency on MLT (van de Kamp et al., 2018). The simulations are made

with a variant of the Whole Atmosphere Community Climate Model, WACCM-D, which includes mesospheric chemistry of

positive and negative ions and is designed for particle precipitation studies in the mesosphere and upper stratosphere (Verronen
60   et al., 2016). This allows for detailed simulations of the ion-neutral chemistry interaction leading to HO_x production, in contrast
to simple parameterizations that are typically used. We analyse monthly mean results as well as monthly averages at different
local times, and discuss the differences in the ozone impact in the context of overall uncertainties in the MEE forcing.

2   Model and Simulations

Here we use CESM version 1.0.5 with WACCM-D, similar to the setup used by Andersson et al. (2016). Our WACCM
65   version is 4, for more details on the model see Marsh et al. (2013). The model was run at $1.95° \times 2.5°$ latitude×longitude
resolution with 88 pressure levels between the ground and the top altitude of 6×10^{-6} hPa ($\approx$140 km). The specified dynamics
configuration was used, i.e. surface pressure and horizontal winds and temperatures up to 50 km were taken from NASA's
Modern-Era Retrospective Analysis for Research and Applications (MERRA) (Rienecker et al., 2011). Standard EPP input
includes precipitation in the auroral regions by electrons with a characteristic energy of 2 keV and a Maxwellian energy
70   distribution as well as ionization due to solar protons at energies between 1 and 300 MeV. In addition, we apply ionization due
to galactic cosmic rays from the NAIRAS model as described by Jackman et al. (2016).

For the radiation belt electron precipitation, we used the APEEP proxy model version 2 by van de Kamp et al. (2018). Fitted
to satellite-based electron observations and using the geomagnetic Ap index as the sole driver, APEEP provides integrated
electron fluxes above 30 keV energy and energy-flux gradients at McIlwain L shells between 2 and 10, i.e. between $44°$ and
75   $72°$ of magnetic latitude. This latitude region is primarily influenced by electrons from the outer Van Allen radiation belt (e.g.
Baker et al., 2018). APEEPv2 can output daily zonal averages or daily averages for eight MLT sectors. Compared to the earlier
version 1 (van de Kamp et al., 2016), APEEPv2 applies a more conservative noise floor screening for satellite data and provides,
in addition to daily zonal means, daily MLT-dependent output over eight three-hour sectors. The purpose of the APEEP models
is to allow for multi-decadal climate simulations with electron forcing, e.g. APEEPv1 atmospheric ionization rates are included
80   in the solar forcing recommendation of the Coupled Model Intercomparison Project Phase 6 (CMIP6), as described in Matthes
et al. (2017). For the purpose of this study, the new provision is MLT-dependent MEE ionization production rates. Figure 1
shows ionization rates at 88 km altitude from APEEPv2 for the period between 1998 and 2012. The variation with solar activity
is clear, with the lowest ionization seen in 2009 during the solar minimum. The strongest ionization is in the declining phase
of solar cycle, peaking in 2003. The ionization typically maximises at magnetic latitudes $60°$ –$70°$.

85   We performed WACCM-D simulations using three different APEEP ionization inputs: 1) no input (Zero), 2) APEEPv2
zonal mean (ZM), and 3) APEEPv2 MLT-dependent (MLT). Note that we calculated APEEPv2 zonal mean ionization from
APEEPv2 MLT ionization to make sure that the daily total energy input is the same for simulations with input 2 and 3. Two
cases were selected: year 2003 for high APEEP impact, and Extreme Case. For the Extreme Case, high APEEP ionization on
7 March 2005 of was first multiplied by factor of 10 at all altitudes and L shells, and then applied constantly in a three-month
90   simulation from January to March 2002. The Extreme Case is thus somewhat arbitrary but nevertheless useful for verifying
the 2003 results with a very strong and perpetual MEE forcing. Ionization rates for the extreme case are shown in Figure 2 on

the WACCM latitude-longitude grid at an altitude of $\approx$75 km. MLT is defined as the magnetic longitude from the midnight magnetic meridian, converted to hours at 1 hour per $15°$. The difference in forcing between zonal mean and MLT-dependent forcing is clear, MLT ionization is strongest in the early morning-to-noon sector and has a minimum in early afternoon. During each 24 hours of simulation, these patterns rotate once around the pole, at each time step following MLT. Even at this relatively low altitude, the zonal mean ionization rate reaches 2000 $\text{cm}^{-3}\text{s}^{-1}$ in the middle of the radiation belt latitudes, while the 2003 mean at the same altitude and latitude is about 65 $\text{cm}^{-3}\text{s}^{-1}$ (not shown).

3 Results

Obviously, the MLT-dependent forcing produces results that should have differences to those from the ZM forcing if we looked at hourly output from WACCM-D. This particularly applies to species which have short chemical lifetimes, such as the ions. For some neutral species, like HO_x, the APEEP-driven differences in production are partly masked by background diurnal variability of chemical production and loss, and are not seen as clearly as in the ionization rates shown in Figure 2.

However, since the APEEP models are designed to be used in multi-decadal climate simulations such as those conducted during CMIP6, it is more interesting to ask if the analysis of such simulations gives different answers if MLT-dependent APEEP forcing is applied. Typically, long climate simulations are analyzed using monthly mean data. Thus we concentrate on WACCM-D monthly mean output first. Then, we also consider different local times (LSTs) separately from hourly output data saved separately. This would be similar to analysis of data from polar orbiting satellites, such measurements are typically made at limited local times for any given latitude.

Ozone changes caused by EPP have been suggested to drive the top-down dynamical coupling between middle atmosphere and troposphere. Thus we start our analysis directly with ozone, and then go on to ozone-affecting NO_x and HO_x. Polar cap means shown in the following Sections were calculated as area-weighted (cosine-of-latitude scaling) averages at geographic latitudes $60°-90°$. We concentrate more on the SH, because there geomagnetic latitudes span over a wider range of geographic latitudes than in the NH and thus cover a wider range of background conditions and diurnal variability, especially during winter. Thus we can expect that, overall, the MLT dependency of APEEP forcing should be more important factor in the SH atmosphere.

3.1 Ozone

Figure 3 shows the monthly mean results for SH polar cap in year 2003. In Figure 3a, the impact of MLT-dependent APEEP forcing on mesospheric ozone is strongest, with up to $\approx$10% depletion, between April and September at pressure levels between 0.1 and 0.01 hPa. The depletion is caused by increased HO_x production. In the stratosphere, depletion up to $\approx$3% is seen from June to October, descending from 1 to 10 hPa. The stratospheric depletion and the descent are both caused by increased NO_x descending inside the polar vortex from production region in the mesosphere-lower thermosphere towards lower altitudes. The APEEP effects are moderate in October and November due to the major effect from the great Halloween solar proton event (e.g. Funke et al., 2011) which is included in all simulations. Above 0.01 hPa, the ozone effect becomes less consistent, i.e.

small increases and decreases are both seen, partly due to atomic oxygen increase affecting its balance with ozone. Overall and

125 qualitatively, our results agree well with results from an ensemble of multi-decadal simulations using free-running dynamics (e.g. Andersson et al., 2018).

Figure 3b shows the impact of ZM APEEP forcing on ozone. The magnitude and extent of the response is clearly very similar to the response to MLT-dependent forcing shown in Figure 3a. For a more detailed view, Figure 3c shows the relative difference between simulations using the MLT and ZM APEEP forcing. APEEP Zero is used as a reference here, as it was in panels (a)

130 and (b), so that the percentage numbers in the three panels are directly comparable. The main response patterns below 0.01 hPa in panels (a) and (b) are not seen in panel (c), which indicates that applying MLT-dependency has little effect for the monthly mean ozone impact. Around the 0.01 hPa ozone minimum, there is a region with relative increases and decreases by a few percent.

In the following, we selected August 2003 for a closer study of effects at different LST. As seen in Figure 3, August has a

135 clear APEEP impact in both the mesosphere and upper stratosphere. The LST analysis results for other months (not shown) are qualitatively similar to the August results but depend on overall APEEP impact in each month.

Figure 4 shows the LST mean results for SH polar cap in August 2003. In other words, eight LST sectors (three hours each) have been averaged separately over the entire month. Data in each sector are similar to what would be available from satellite instruments which measure at limited local times at each latitude. In Figure 4a, impact of APEEP MLT is seen in basically

140 three altitude stripes across all LST. Between 1 and 10 hPa, the depletion of ozone due to descending NO_x is not dependent on the LST, and there is no clear diurnal variability of background ozone either (Figure 4d). From 0.1 to 0.01 hPa, the daytime depletion is at slightly lower altitude range than at night. However, this is mostly related to the diurnal variability of ozone concentration at these altitudes (Figure 4d). Around 0.001 hPa, a few percent of increase is seen especially at nighttime. The increase comes from production of atomic oxygen, with a lower production from MLT-dependent forcing at noon-afternoon

145 sectors. The APEEP contribution is also less important in the daytime when solar EUV dissociates oxygen molecules for ozone production.

The response to ZM APEEP forcing is shown in Figure 4b, and it is again very similar to the response to MLT-dependent forcing. Figure 4c, shows the relative difference between simulations using the APEEP MLT and APEEP ZM forcing. Around 0.001 hPa, MLT forcing depletes 1–2% more ozone than ZM forcing at all LST. This is particularly seen in the early morning

150 hours when MLT forcing produces more atomic oxygen than ZM. This effect reaches down to the 0.01 hPa ozone minimum. At 0.1–0.01 hPa, the MLT forcing adds to the ozone depletion by a few percent consistently at all LST compared to ZM, which is a minor difference when compared to the 7–15% impact seen in Panels (a) and (b) of Figure 4. Both MLT and ZM produce largest depletion from midnight to early morning. In the stratosphere, the differences are less than 1%.

Figure 5 shows an example of our results from the Extreme Case, the data shown are monthly zonal means for February. Here

155 we look at the MEE forcing region only, i.e. the mesosphere and above, because the three-month span of this simulation is not long enough for NO_x transport to cause full stratospheric effects. The ozone impacts below 0.1 hPa are thus small (not shown). Although both hemispheres were equally forced with APEEP, except for the differences in the geographic extent of magnetic latitudes, the ozone effect is much clearer in the NH winter pole (Panels 5a and 5b) due to faster recovery in the summer pole

through production driven by O_2 photodissociation. Depletion is seen at an altitude range between 0.01 and 0.5 hPa at latitudes
$45° − 90°$ degrees, with the strongest effect reaching 45% just below 0.01 hPa and North of $60°$. The depletion here is naturally
stronger than for the year 2003 because the extreme APEEP forcing was applied throughout the simulation. The response
extends down to latitude $≈ 45°$, which is consistent with the extent of the APEEP forcing (see Figure 2). The simulations with
ZM and MLT forcings give very similar results, and the differences are generally marginal in the range of a few percent, except
in few small and isolated regions.

3.2 Odd nitrogen

Odd nitrogen (NO_x) chemical lifetime is days-to-months in the mesosphere-lower thermosphere, and NO_x concentration can
easily accumulate especially during polar winter conditions. Therefore, one would expect that a faithful representation of MLT
dependency of APEEP forcing and NO_x production is probably not crucial for the NO_x distribution or NO_x-driven ozone
depletion in the upper stratosphere.

Figure 6 shows the monthly zonal mean results for February from the Extreme Case. Largest increases, reaching up to and
beyond an order of magnitude, are seen between 0.1 and 0.001 hPa at polar latitudes, i.e. at the latitudes and altitudes where
the APEEP forcing is applied. The increase extends from polar regions to all latitudes, the mid and low latitudes outside the
forcing region showing a smaller but still $> 100\%$ impact in large regions. The SH effect is relatively stronger in magnitude
than the NH effect due to the lower background concentration there. In the NH, the beginning effect of NO_x descend inside
the polar vortex extends the impact towards the stratopause. The MLT and ZM forcings produce again a very similar response,
in both magnitude and spatial extent, and the differences are small compared to the overall effect. However, the MLT forcing
results in up to 1/10 less NO_x in the peak response regions around 0.01 hPa than the ZM forcing, except at the very poles. At
pressure levels below 0.05 hPa and above 0.003 hPa the relative differences are smaller.

Figure 7 shows the monthly mean results for SH polar cap in year 2003. In summer months, the APEEP forcing enhances
NO_x down to the middle mesosphere only, due to lack of downward transport combined with efficient loss from solar pho-
todissociation. During winter months, when less radiation is available and chemical lifetime of NO_x increases, NO_x created by
APEEP above 0.1 hPa descends inside the polar vortex towards the stratospheric altitudes. Relatively, the NO_x enhancement is
strongest during autumn and spring times, due to combination of lower solar photodissociation and lower background concen-
tration than in the summer and winter, respectively. Figure 7 results agree qualitatively well with results from a multi-decadal
ensemble of simulations using WACCM with free-running dynamics (e.g. Andersson et al., 2018). The differences between the
response to APEEP MLT and ZM are rather small. In general, the differences in resulting NO_x concentration are less than 1/10,
except in July around 0.2 hPa. In autumn and early winter, MLT forcing results in a smaller NO_x response in the mesosphere
compared to ZM forcing, while in late winter the MLT forcing produces more NO_x in the lower mesosphere.

3.3 Odd hydrogen

Odd hydrogen (HO_x) production from H_2O by APEEP ionization is restricted to altitudes below 0.01 hPa ($≈80$ km), due to
the small amount H_2O available for ion chemistry at altitudes above. This is clearly seen in Figure 8a which shows the monthly

zonal mean response to APEEP MLT for February from the Extreme Case: there is no clear response above 0.01 hPa at any latitude. Also, the SH summer pole shows little effect due to APEEP contribution being less than that from solar Lyman-α photodissociation of H_2O. In the NH winter pole, the largest region of HO_x increase is at 0.1–0.01 hPa and latitudes between 195 $40°$ and $80°$, i.e. exactly in the region of direct APEEP forcing. In contrast, a clear decrease is seen below 0.04 hPa at high latitudes above $80°$, in a region where HO_x background concentration is very small. This happens outside the APEEP HO_x production region, and seems to be a chemical response to to enhanced NO_x, similar to the decrease in HO_x at 45–60 km shown by Verronen and Lehmann (2015) in their Figure 1.

4   Discussion

200   Our results indicate that the MLT-dependent diurnal variability of MEE forcing can be ignored without causing large differences in simulated ozone response when analysed on monthly time scales. The same conclusion applies to monthly averages calculated at individual local times. When comparing simulations with daily zonal average MEE and MLT-dependent MEE, differences in the magnitude of the response do exist but they are not more than a few percent for ozone. Spatial patterns of response are very similar between the simulations. Thus, the lack of MLT-dependency in the current CMIP6 MEE forcing data 205   should not create any important uncertainty in long-term climate simulations.

Our simulations use specified dynamics up to 50 km altitude. In the stratosphere, the small chemical differences between the simulations suggest that any differences in dynamics or dynamical feedback would also be small. Above 50 km, our simulations are dynamically free running. In general, the specified dynamics below 50 km control much of the dynamics at altitudes above as well. Thus, dynamical differences between simulations using specified dynamics should be much smaller than between 210   fully-free-running simulations. Nevertheless, as seen in Figure 3c for ozone, the relative differences between the APEEP MLT and APEEP ZM simulations above 0.1 hPa ($\approx$60 km) increase from < 1% to up to 2–4% around 0.01 hPa, are smaller around 0.001 hPa, and then increase again around 0.0001 hPa. Although part of this increase in relative differences comes from smaller background values of ozone than at altitudes below (see Figure 3d), there should also be a contribution from the free-running dynamics. To quantify this contribution we made a 10-member ensemble simulation of year 2003, with specified dynamics and 215   APEEP Zero forcing. From this ensemble, we calculated the standard deviation of monthly mean polar cap anomalies (N = 10), individually for each month, and show them for the SH in Figure 9. Below 0.1 hPa, i.e. at altitudes where specified dynamics are applied, STD is always below 0.5%. Above, there are two STD maxima around 0.01 and 0.0001 hPa, on average 1.5–2% and reaching up to 3–4% in winter months. These maxima coincide with the increased ozone differences seen in Figure 3c, with a similar magnitude. Thus the ozone differences between simulations, seen when using different MLT-dependency of the 220   applied APEEP forcing, are within the statistical variability coming from free-running model dynamics and are not significant.

To put the uncertainties caused by MEE MLT dependency into a wider context, Figure 10 shows a SH ozone impact comparison between simulations using zonal mean forcing from APEEPv1 and APEEPv2 for the year 2003. The ozone impact from APEEPv1 is, in general, about twice as large as that from APEEPv2. This is seen for the mesospheric HO_x-driven depletion in mid winter as well as for the springtime NO_x-driven depletion in the upper stratosphere. The difference in ozone

225 impact is a result of lower ionization rates in APEEPv2, caused by a more careful consideration of the MEPED instrument noise floor (van de Kamp et al., 2018). Further, recent studies have demonstrated that flux uncertainties related to MEPED electron flux measurements, which the APEEP models are based on, can reach an order of magnitude in certain conditions and particularly for low fluxes (Nesse Tyssøy et al., 2019). It seems thus clear that the impact of uncertainties related to electron flux observations greatly exceeds those related to the MLT dependency applied in atmosphere and climate simulations.

230   Our conclusions are for the monthly mean atmospheric impact caused by MEE: we showed that ignoring the MLT dependency does not create significant differences in simulations. Our conclusions do not apply as such for atmospheric impacts in daily or hourly time scales but these should be studied separately. Finally, it is important to note that a good MLT coverage is a crucial factor when making MEE flux observations because of the order-of-magnitude variability with MLT (e.g. in Figure 2). Even when atmospheric simulations can be made with zonal mean MEE forcing, it is important to apply a forcing that provides

235 correct amount of total energy input and this requires flux measurements that have an adequate MLT coverage. Nevertheless, assessment of ozone and NO_x responses does not need complete MLT coverage, which eases the observational requirements for any new atmospheric instrument or existing datasets.

Code and data availability. All model data used are available from corresponding author by request (pekka.verronen@oulu.fi). CESM source code is distributed freely through a public subversion code repository (http://www.cesm.ucar.edu/models/cesm1.0/). WACCM-D has

240 been officially released with the CESM version 2.0 in June 2018 (http://www.cesm.ucar.edu/models/cesm2/).

Competing interests. The authors declare that no competing interests are present.

Acknowledgements. The authors would like to thank the CHAMOS group (http://chamos.fmi.fi) for useful discussions. This material is based upon work supported in part by the National Center for Atmospheric Research, which is a major facility sponsored by the National Science Foundation under Cooperative Agreement No. 1852977. DRM is also supported by NSF Award #1650918 "Collaborative Research: CEDAR

245 - Quantifying the Impact of Radiation Belt Electron Precipitation on Atmospheric Reactive Nitrogen Oxides (NO_x) and Ozone (O_3)".

References

Aikin, A. C. and Smith, H. J. P.: Mesospheric constituent variations during electron precipitation events, J. Geophys. Res., 104, 26 457–26 472, 1999.

Andersson, M. E., Verronen, P. T., Rodger, C. J., Clilverd, M. A., and Seppälä, A.: Missing driver in the Sun-Earth connection from energetic electron precipitation impacts mesospheric ozone, Nature Commun., 5, https://doi.org/10.1038/ncomms6197, 2014.

Andersson, M. E., Verronen, P. T., Marsh, D. R., Päivärinta, S.-M., and Plane, J. M. C.: WACCM-D – Improved modeling of nitric acid and active chlorine during energetic particle precipitation, J. Geophys. Res. (Atmos.), 121, 10,328–10,341, https://doi.org/10.1002/2015JD024173, 2016.

Andersson, M. E., Verronen, P. T., Marsh, D. R., Seppälä, A., Päivärinta, S.-M., Rodger, C. J., Clilverd, M. A., Kalakoski, N., and van de Kamp, M.: Polar Ozone Response to Energetic Particle Precipitation Over Decadal Time Scales: The Role of Medium-Energy Electrons, J. Geophys. Res. (Atmos.), 123, 607–622, https://doi.org/10.1002/2017JD027605, 2018.

Baker, D. N., Erickson, P. J., Fennell, J. F., Foster, J. C., Jaynes, A. N., , and Verronen, P. T.: Space weather effects in the Earth's radiation belts, Space Sci. Rev., 214:17, https://doi.org/10.1007/s11214-017-0452-7, 2018.

Callis, L. B. and Lambeth, J. D.: NO_y formed by precipitating electron events in 1991 and 1992: Descent into the stratosphere as observed by ISAMS, Geophys. Res. Lett., 25, 1875–1878, https://doi.org/10.1029/98GL01219, 1998.

Damiani, A., Funke, B., Santee, M. L., Cordero, R. R., and Watanabe, S.: Energetic particle precipitation: A major driver of the ozone budget in the Antarctic upper stratosphere, Geophys. Res. Lett., 43, 3554–3562, https://doi.org/10.1002/2016GL068279, 2016.

Funke, B., López-Puertas, M., Gil-Lopez, S., von Clarmann, T., Stiller, G. P., Fischer, H., and Kellmann: Downward transport of upper atmospheric NOx into the polar stratosphere and lower mesosphere during the Antarctic 2003 and Arctic 2002/2003 winters, J. Geophys. Res., 110, D24 308, https://doi.org/10.1029/2005JD006463, 2005.

Funke, B., Baumgaertner, A., Calisto, M., Egorova, T., Jackman, C. H., Kieser, J., Krivolutsky, A., López-Puertas, M., Marsh, D. R., Reddmann, T., Rozanov, E., Salmi, S.-M., Sinnhuber, M., Stiller, G. P., Verronen, P. T., Versick, S., von Clarmann, T., Vyushkova, T. Y., Wieters, N., and Wissing, J. M.: Composition changes after the "Halloween" solar proton event: the High-Energy Particle Precipitation in the Atmosphere (HEPPA) model versus MIPAS data intercomparison study, Atmos. Chem. Phys., 11, 9089–9139, https://doi.org/10.5194/acp-11-9089-2011, 2011.

Fytterer, T., Mlynczak, M. G., Nieder, H., Pérot, K., Sinnhuber, M., Stiller, G., and Urban, J.: Energetic particle induced intra-seasonal variability of ozone inside the Antarctic polar vortex observed in satellite data, Atmos. Chem. Phys., 15, 3327–3338, https://doi.org/10.5194/acp-15-3327-2015, http://www.atmos-chem-phys.net/15/3327/2015/, 2015.

Horne, R. B., Lam, M. M., and Green, J. C.: Energetic electron precipitation from the outer radiation belt during geomagnetic storms, Geophys. Res. Lett., 36, L19 104, https://doi.org/10.1029/2009GL040236, 2009.

Jackman, C. H., Marsh, D. R., Kinnison, D. E., Mertens, C. J., and Fleming, E. L.: Atmospheric changes caused by galactic cosmic rays over the period 1960–2010, Atmos. Chem. Phys., 16, 5853–5866, https://doi.org/10.5194/acp-16-5853-2016, 2016.

Marsh, D. R., Mills, M., Kinnison, D., Lamarque, J.-F., Calvo, N., and Polvani, L.: Climate change from 1850 to 2005 simulated in CESM1(WACCM), J. Climate, 26, 7372–7391, https://doi.org/10.1175/JCLI-D-12-00558.1, 2013.

Matthes, K., Funke, B., Andersson, M. E., Barnard, L., Beer, J., Charbonneau, P., Clilverd, M. A., Dudok de Wit, T., Haberreiter, M., Hendry, A., Jackman, C. H., Kretschmar, M., Kruschke, T., Kunze, M., Langematz, U., Marsh, D. R., Maycock, A., Misios, S., Rodger, C. J.,

Scaife, A. A., Seppälä, A., Shangguan, M., Sinnhuber, M., Tourpali, K., Usoskin, I., van de Kamp, M., Verronen, P. T., and Versick, S.: Solar Forcing for CMIP6, Geosci. Model Dev., 10, 2247–2302, https://doi.org/10.5194/gmd-10-2247-2017, 2017.

Nesse Tyssøy, H., Haderlein, A., Sandanger, M. I., and Stadsnes, J.: Intercomparison of the POES/MEPED loss cone electron fluxes with the
285   CMIP6 parametrization, J. Geophys. Res. (Space Phys.), 124, 628–642, https://doi.org/10.1029/2018JA025745, 2019.

Päivärinta, S.-M., Verronen, P. T., Funke, B., Gardini, A., Seppälä, A., and Andersson, M. E.: Transport versus energetic particle precipitation: Northern polar stratospheric NO_x and ozone in January-March 2012, J. Geophys. Res. (Atmos.), 121, 6085–6100, https://doi.org/10.1002/2015JD024217, 2016.

Randall, C. E., Harvey, V. L., Siskind, D. E., France, J., Bernath, P. F., Boone, C. D., and Walker, K. A.: NO_x descent in the Arctic middle
290   atmosphere in early 2009, Geophys. Res. Lett., 36, L18 811, https://doi.org/10.1029/2009GL039706, 2009.

Rienecker, M. M., Suarez, M. J., Gelaro, R., Todling, R., Bacmeister, J., Liu, E., Bosilovich, M. G., Schubert, S. D., Takacs, L., Kim, G.-K., Bloom, S., Chen, J., Collins, D., Conaty, A., da Silva, A., Gu, W., Joiner, J., Koster, R. D., Lucchesi, R., Molod, A., Owens, T., Pawson, S., Pegion, P., Redder, C. R., Reichle, R., Robertson, F. R., Ruddick, A. G., Sienkiewicz, M., and Woollen, J.: MERRA: NASA's Modern-Era Retrospective Analysis for Research and Applications, J. Climate, 24, 3624–3648, https://doi.org/10.1175/JCLI-D-11-00015.1, 2011.

295 Siskind, D. E., Nedoluha, G. E., Randall, C. E., Fromm, M., and Russell III, J. M.: An assessment of Southern Hemisphere stratospheric NO_x enhancements due to transport from the upper atmosphere, Geophys. Res. Lett., 27, 329–332, 2000.

Solomon, S., Rusch, D. W., Gérard, J.-C., Reid, G. C., and Crutzen, P. J.: The effect of particle precipitation events on the neutral and ion chemistry of the middle atmosphere: II. Odd hydrogen, Planet. Space Sci., 8, 885–893, 1981.

van de Kamp, M., Seppälä, A., Clilverd, M. A., Rodger, C. J., Verronen, P. T., and Whittaker, I. C.: A model providing long-
300   term datasets of energetic electron precipitation during geomagnetic storms, J. Geophys. Res. (Atmos.), 121, 12 520–12 540, https://doi.org/10.1002/2015JD024212, 2016.

van de Kamp, M., Rodger, C. J., Seppälä, A., Clilverd, M. A., and Verronen, P. T.: An updated model providing long-term datasets of energetic electron precipitation, including zonal dependence, J. Geophys. Res. (Atmos.), 123, 9891–9915, https://doi.org/10.1029/2017JD028253, https://doi.org/10.1029/2017JD028253, 2018.

305 Verronen, P. T. and Lehmann, R.: Analysis and parameterisation of ionic reactions affecting middle atmospheric HO_x and NO_y during solar proton events, Ann. Geophys., 31, 909–956, https://doi.org/10.5194/angeo-31-909-2013, 2013.

Verronen, P. T. and Lehmann, R.: Enhancement of odd nitrogen modifies mesospheric ozone chemistry during polar winter, Geophys. Res. Lett., 42, 10,445–10,452, https://doi.org/10.1002/2015GL066703, 2015.

Verronen, P. T., Seppälä, A., Clilverd, M. A., Rodger, C. J., Kyrölä, E., Enell, C.-F., Ulich, T., and Turunen, E.: Diurnal variation of ozone
310   depletion during the October-November 2003 solar proton events, J. Geophys. Res., 110, A09S32, https://doi.org/10.1029/2004JA010932, 2005.

Verronen, P. T., Seppälä, A., Kyrölä, E., Tamminen, J., Pickett, H. M., and Turunen, E.: Production of odd hydrogen in the mesosphere during the January 2005 solar proton event, Geophys. Res. Lett., 33, L24 811, https://doi.org/10.1029/2006GL028115, 2006.

Verronen, P. T., Andersson, M. E., Marsh, D. R., Kovács, T., and Plane, J. M. C.: WACCM-D – Whole Atmosphere Community Climate
315   Model with D-region ion chemistry, J. Adv. Model. Earth Syst., 8, 954–975, https://doi.org/10.1002/2015MS000592, 2016.

Whittaker, I. C., Clilverd, M. A., and Rodger, C. J.: Characteristics of precipitating energetic electron fluxes relative to the plasmapause during geomagnetic storms, J. Geophys. Res. (Space Phys.), 119, 8784–8800, https://doi.org/10.1002/2014JA020446, 2014.
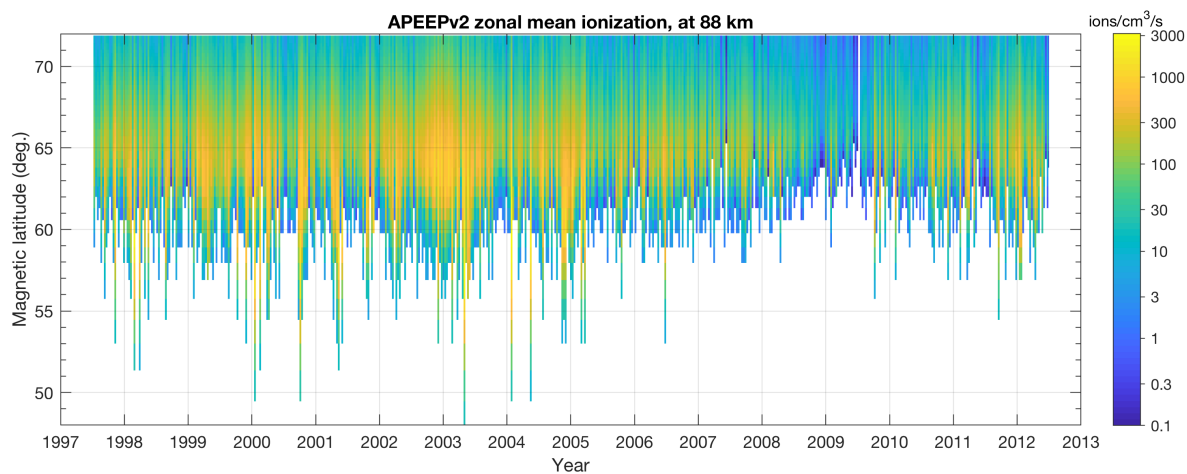
Figures

Figure 1. Ionization rates from the APEEPv2 model. The daily data have been averaged into 10-day resolution for clarity. The white areas indicate no data and correspond to satellite flux measurements that were screened for being below the noise floor. X axis tick marks are in the middle of each year.
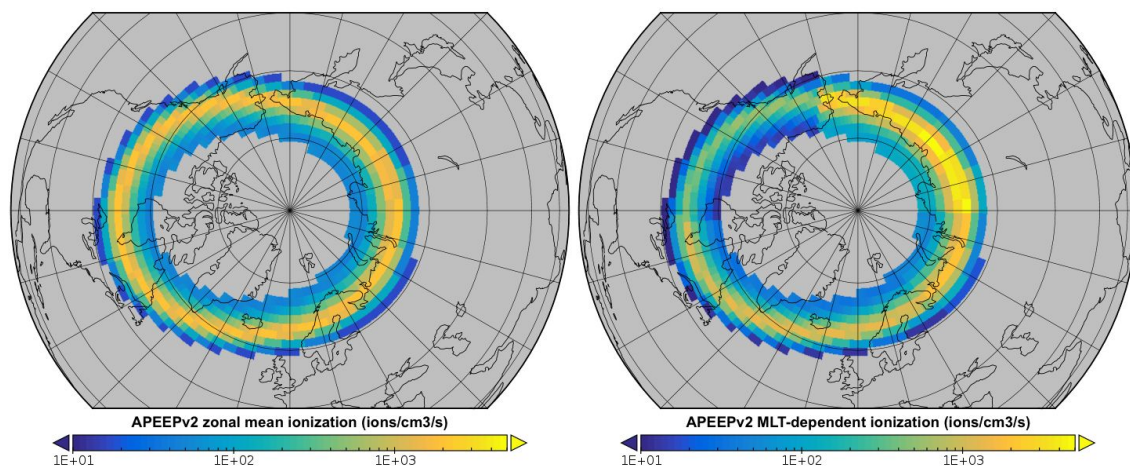
Figure 2. Extreme Case ionization rates at approximative altitude 75 km (0.0264 hPa) and midnight UT presented on the WACCM-D geographic latitude-longitude grid. (left) APEEPv2 zonal mean forcing. (right) APEEPv2 MLT-dependent forcing over eight three-hour sectors. Gray areas have no APEEP forcing.
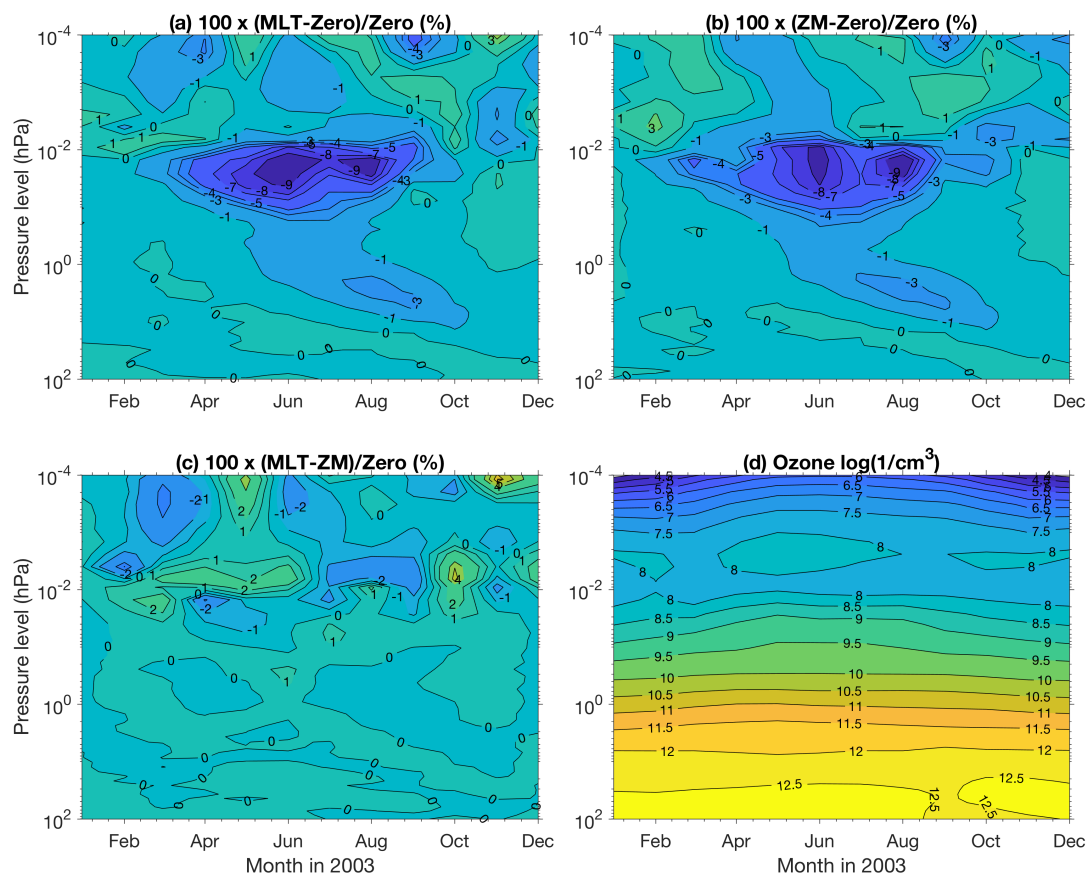
Figure 3. SH polar cap ozone, monthly means for the year 2003. (a) 100×(MLT-Zero)/Zero, i.e. relative differences between simulations using MLT-dependent and Zero APEEP forcing, (b) 100×(ZM-Zero)/Zero, i.e. relative differences between simulations using zonal mean and Zero APEEP forcing, (c) 100×(MLT-ZM)/Zero, i.e. relative differences between simulations using MLT-dependent and zonal mean APEEP forcing, (d) 10-based logarithm of ozone concentrations from simulations with MLT-dependent APEEP.
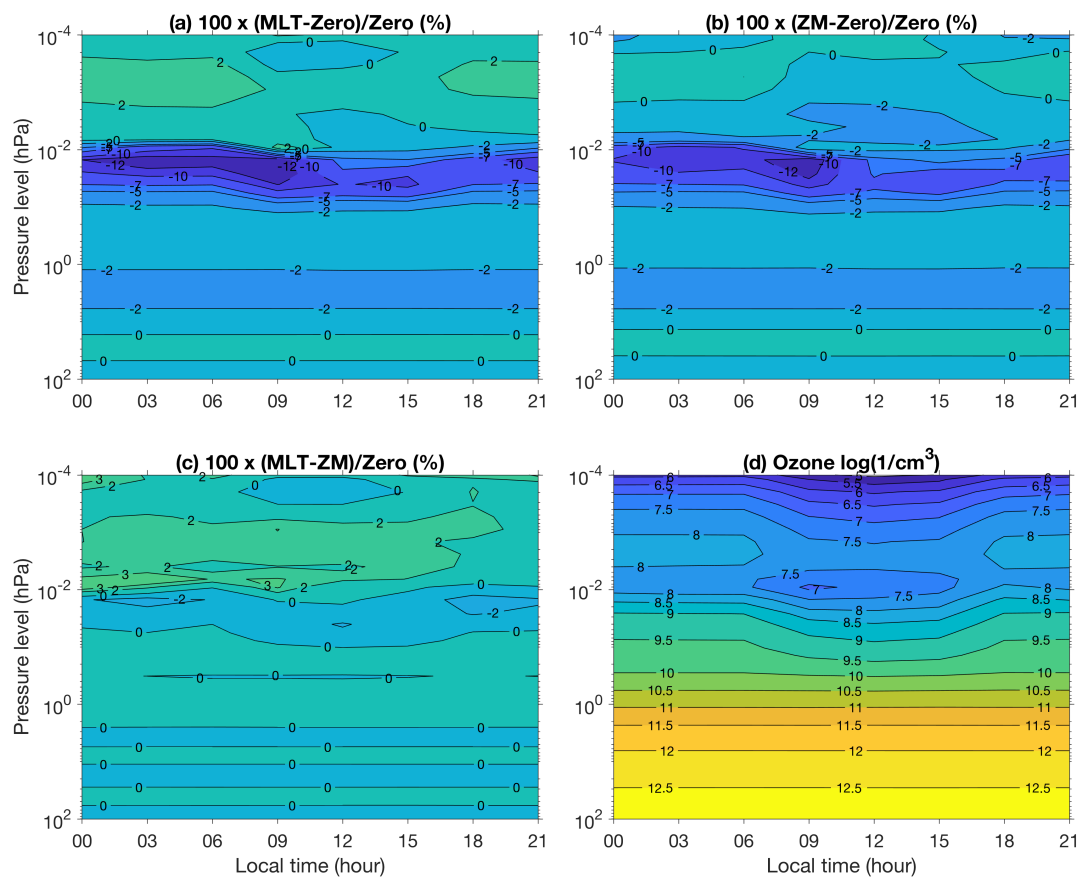
Figure 4. SH polar cap ozone, LST means for August 2003. (a) relative differences between simulations using MLT-dependent and Zero APEEP forcing, (b) relative differences between simulations using ZM and Zero APEEP forcing, (c) relative differences between simulations using MLT-dependent and ZM MEE forcing, (d) 10-based logarithm of ozone concentrations from the simulation with MLT-dependent APEEP forcing.
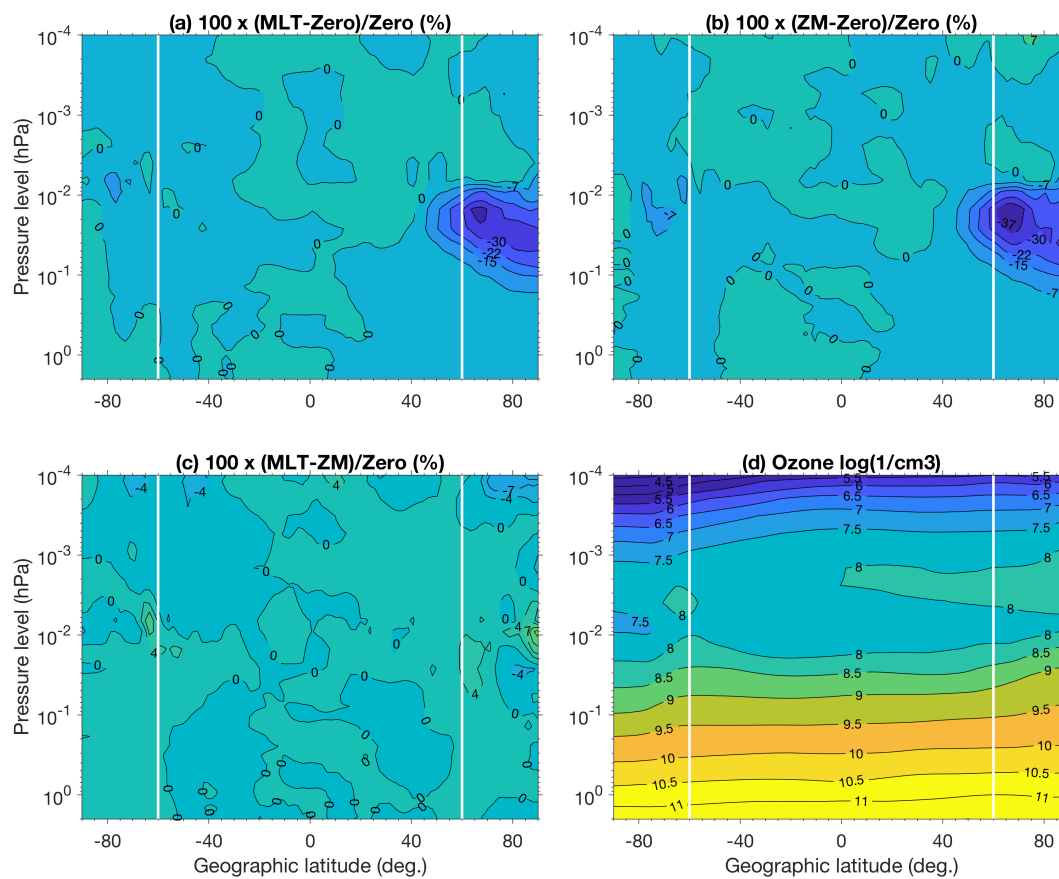
Figure 5. February monthly mean, zonal mean ozone from the Extreme Case simulation. (a) relative differences between simulations using MLT-dependent and zero APEEP forcing, (b) relative differences between simulations using ZM and zero APEEP forcing, (c) relative differences between simulations using MLT-dependent and ZM MEE forcing, (d) 10-based logarithm of ozone concentrations from the simulation with MLT-dependent APEEP forcing. White vertical lines mark the $\pm 60°$ in geographic latitude.
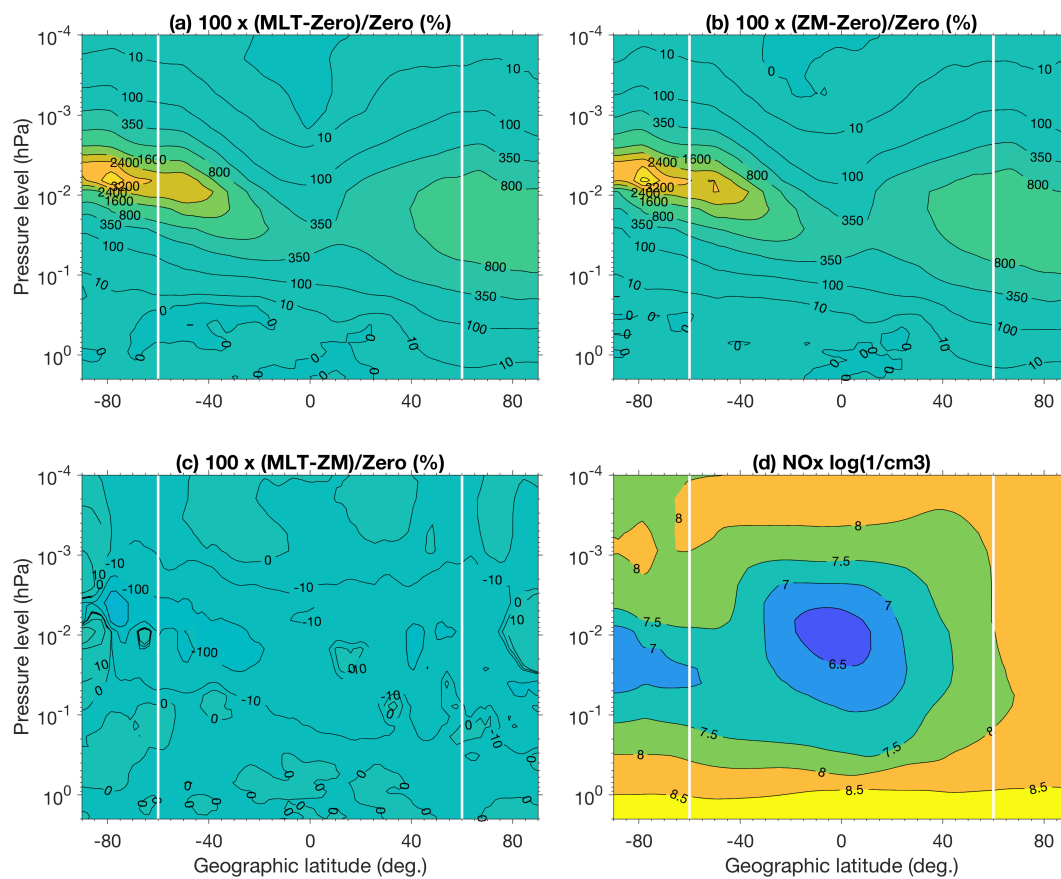
Figure 6. February monthly mean, zonal mean NO_x ($= N + NO + NO_2$) from the Extreme Case simulation. Panels (a)–(d) are as in Figure 5.
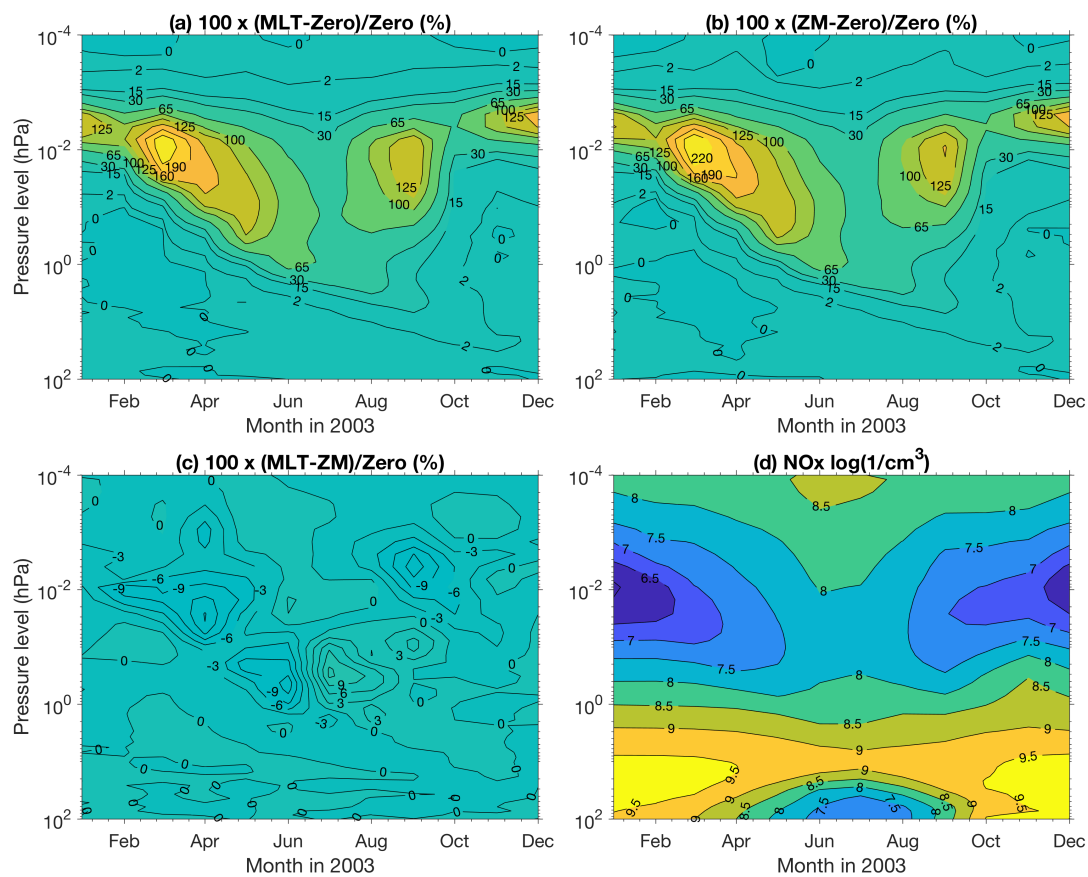
Figure 7. SH polar cap NO_x, monthly means for year 2003. Panels (a)–(d) are as in Figure 3.
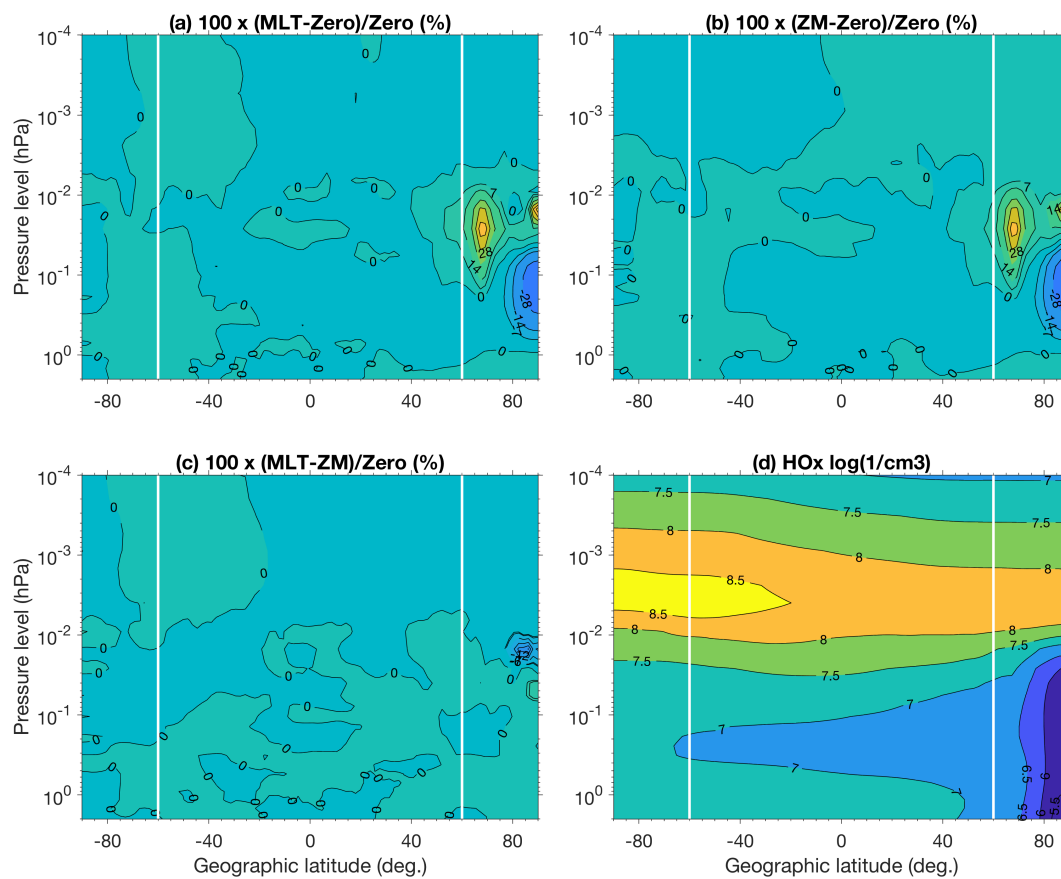
Figure 8. February monthly mean, zonal mean HO_x (= H + OH + HO_2) from the Extreme Case simulation. Panels (a)–(d) are as in Figure 5.
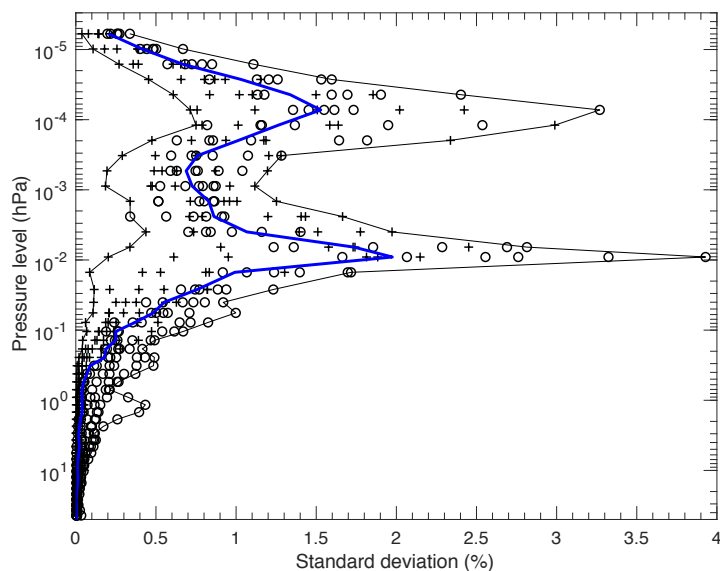
Figure 9. Standard deviation (STD) of the Southern Hemisphere polar cap monthly ozone anomalies from a 10-member ensemble of SD-WACCM-D APEEP Zero simulations, relative to the ensemble mean. Plusses show STD for individual months of January, February, March, October, November and December (summer), circles are for individual months from April to September (winter), black lines indicate the minimum and maximum STD at each pressure level, and the blue thick line is the median of all monthly STDs.
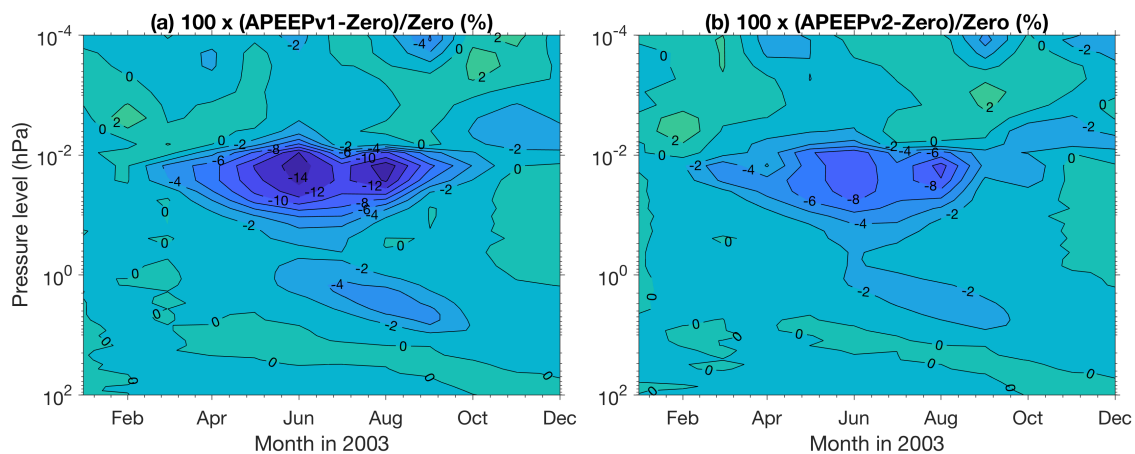
Figure 10. SH polar cap ozone, monthly means for the year 2003. (a) $100\times$(APEEPv1-Zero)/Zero, i.e. relative differences between simulations using Version 1 and Zero APEEP forcing, (b) $100\times$(APEEPv2-Zero)/Zero, i.e. relative differences between simulations using Version 2 and Zero APEEP forcing. Note that Panel (b) shows the same data as Figure 3b but the contour lines are different.